Received 10 April 2022
Revised 12 April 2022
Accepted 12 April 2022

Distribution characteristics and the evolution law of excavation damage zone in the large-span transition section of high-speed railway tunnel based on microseismic monitoring

Ao Li
Urban Construction and Rail Transit Design Institute, JSTI Group, Nanjing, China
Dingli Zhang and Zhenyu Sun
School of Civil Engineering, Beijing Jiaotong University, Beijing, China, and
Jun Huang and Fei Dong
Urban Construction and Rail Transit Design Institute, JSTI Group, Nanjing, China

Abstract

Purpose – The microseismic monitoring technique has great advantages on identifying the location, extent and the mechanism of damage process occurring in rock mass. This study aims to analyze distribution characteristics and the evolution law of excavation damage zone of surrounding rock based on microseismic monitoring data.

Design/methodology/approach – *In situ* test using microseismic monitoring technique is carried out in the large-span transition tunnel of Badaling Great Wall Station of Beijing-Zhangjiakou high-speed railway. An intelligent microseismic monitoring system is built with symmetry monitoring point layout both on the mountain surface and inside the tunnel to achieve three-dimensional and all-round monitoring results.

Findings – Microseismic events can be divided into high density area, medium density area and low density area according to the density distribution of microseismic events. The positions where the cumulative distribution frequencies of microseismic events are 60 and 80% are identified as the boundaries between high and medium density areas and between medium and low density areas, respectively. The high density area of microseismic events is regarded as the high excavation damage zone of surrounding rock, which is affected by the grade of surrounding rock and the span of tunnel. The prediction formulas for the depth of high excavation damage zone of surrounding rock at different tunnel positions are given considering these two parameters. The scale of the average moment magnitude parameters of microseismic events is adopted to describe the damage degree of surrounding rock. The strong positive correlation and multistage characteristics between the depth of excavation damage zone and deformation of surrounding rock are revealed. Based on the depth of high excavation damage zone of surrounding rock, the prestressed anchor cable (rod) is designed, and the safety of anchor cable (rod) design parameters is verified by the deformation results of surrounding rock.

Originality/value – The research provides a new method to predict the surrounding rock damage zone of large-span tunnel and also provides a reference basis for design parameters of prestressed anchor cable (rod).

Keywords High-speed railway, Large-span tunnel, Excavation damage zone, Microseismic monitoring

Paper type Research paper

This work was supported by the Fundamental Research Funds for Chinese National Natural Science Foundation under Grant 51678035, National Key Research and Development Programs of China under Grant 2017YFC0805401, and China Railway Corporation Research and Development Program of Science and Technology under Grant 2014004-C.

Railway Sciences
Vol. 1 No. 1, 2022
pp. 56-75
Emerald Publishing Limited
e-ISSN: 2755-0915
p-ISSN: 2755-0907
DOI 10.1108/RS-04-2022-0006

1. Introduction

The unloading of tunnel excavation destroys the equilibrium state of natural stress of rock mass and causes the redistribution of surrounding rock stress. When the stress exceeds the bearing capacity of rock mass, microcracks will initiate in the rock mass. The expansion and penetration of microcracks will cause obvious changes in the physical and mechanical properties of rock mass within a certain range around the tunnel excavation face, which are mainly manifested as the decrease of rock mass strength and elastic modulus, and the increase of permeability coefficient (Read, 2004; Sato, Kikuchi, & Sugihara, 2000). The area where the physical and mechanical properties of rock mass change is generally called the excavation damage zone of surrounding rock. With the continuous tunnel excavation, the surrounding rock damage will be further aggravated. If effective supporting measures are not taken in time, the surrounding rock will be unstable and damaged, which will further affect the safety of tunnel construction (Martino & Chandler, 2004; Zhu, Sheng, Zhang, & Li, 2013). Therefore, how to accurately obtain the distribution characteristics and the evolution law of excavation damage zone of surrounding rock becomes a key technical problem to be solved urgently in the engineering, which directly affects the reliability of support and the safety of engineering and has important practical significance and theoretical value (Liu, Zhang, Chu, & Wu, 2013; Liu, Zhang, & Chu, 2015; Cai, Kaiser, & Martin, 2001).

When any crack initiates at the weak position of rock, the energy accumulated in the crack will be released in the form of stress wave, resulting in microseismic/acoustic emission signal. The current microseismic/acoustic emission testing technology can provide real-time information, including the location, degree and size of microcracks and possible destruction process during rock mass damage, and can quickly make qualitative and quantitative evaluation on damage characteristics and development trend of rock mass, which has been successfully applied to some engineering practices (Li, Liu, Zhao, & Yang, 2009; Zhang & Deng, 2016). The Canadian Underground Research Laboratory carried out a series of research studies on excavation damage of surrounding rock through on-site microseismic tests, among which Martin (1997) preliminarily defined the scope of excavation damage zone of surrounding rock through the microseismic event distribution map of Mine-by test tunnel; Martino and Chandler (2004) analyzed the influencing factors of the excavation damage zone of the surrounding rock; Cai and Kaiser (2005) studied the excavation damage degree of surrounding rock based on parameters, such as crack distribution and density, monitored by microseismic monitoring. Chen *et al.* (2010) and Liu, Zhang, Chen, Hou and Chu (2011) conducted an acoustic emission monitoring test during tunnel boring machine (TBM) construction in the deep-buried diversion tunnel of Jinping II Hydropower Station and studied the evolution law of surrounding rock damage during excavation. Li, Shigenori, Koji, Hisaya and Hideo (2001) monitored the acoustic emission of surrounding rock after blasting excavation in the tunnel of Kamiokande underground bedrock test site and analyzed and explained the relaxation phenomenon after tunnel excavation. The above-mentioned microseismic/acoustic emission monitoring technology for research and test on the excavation damage zone of surrounding rock is limited to underground laboratory and hydraulic tunnel, etc. The section is small, and the qualitative research of surrounding rock damage zone is mainly carried out. However, the high speed railway tunnel has a large section, the spatial difference of surrounding rock parameters is significant and the reliability and safety requirements are higher. Therefore, it is necessary to carry out quantitative research on the excavation damage zone of surrounding rock based on the characteristics of large-span high speed railway tunnel.

In this paper, the large-span transition tunnel of Badaling Great Wall Station of the newly-built Beijing-Zhangjiakou high-speed railway is taken as the research object, and microseismic monitoring points are set on the tunnel surface and around the tunnel to construct a three-dimensional and all-round microseismic monitoring system. Through the spatial distribution results of microseismic events, this paper reveals the relationship between

the distribution characteristics of microseismic events and excavation damage zone of surrounding rock, realizes the prediction of excavation damage zone of surrounding rock and provides a new method for the study of excavation damage zone of surrounding rock in large-span tunnel and also provides a basis for the design of anchor cable (rod) support of tunnel.

2. On-site microseismic monitoring of large-span transition tunnel

2.1 Overview of engineering geology

Beijing-Zhangjiakou high-speed railway starts from Beijingbei Railway Station in the east and ends at Zhangjiakou Railway Station in the west, with 11 tunnels and 10 stations in total. The longest tunnel is the New Badaling Tunnel, which is located at the boundary of Changping district and Yanqing district in Beijing. It is a single-barrel double track tunnel with a total length of 12,010 m. Badaling Great Wall Station is an underground station located in the new Badaling Tunnel and also the only underground station in the whole line. It is located in Badaling scenic area and adjacent to the Badaling Great Wall. The main structure of the station is a three-independent barrel small clear distance tunnel, and a large-span single-barrel transition tunnel is set between the two ends of the station and the running tunnel. Five section forms are adopted for the transition tunnel, with a maximum excavation span of 32.7 m and an excavation area of 494.4 m^2. It is the subsurface railway tunnel with the largest excavation span in China at present, with high safety risk and great construction difficulty (Zhang *et al.*, 2018). The plane and section of the large-span transition tunnel (in Zhangjiakou direction) are shown in Figure 1.

Microseismic monitoring is carried out in the large-span transition tunnel in Zhangjiakou direction. In total, 3–4 groups of joints are mainly developed in the rock mass of the monitoring area, the joint spacing is generally 0.1–0.5 m and all of them are closed joints, without any filling in the middle. The rock mass is relatively complete – relatively broken in general. However, the joint fissures develop in the dike contact zone, local joint dense zone, differential weathering zone and alteration zone. Affected by Yanshanian intrusive rocks, the fracture structure in this area is relatively developed. The tunnel trunk crosses F2 fault, intersects with the main tunnel trunk at DK68 + 260–300, intersects with the line by 35° and the fracture occurrence is 236°<80°, which is a compression-torsion fracture. The hanging wall is porphyritic monzonitic granite, the footwall is granite and crushed rock is inside the fault zone.

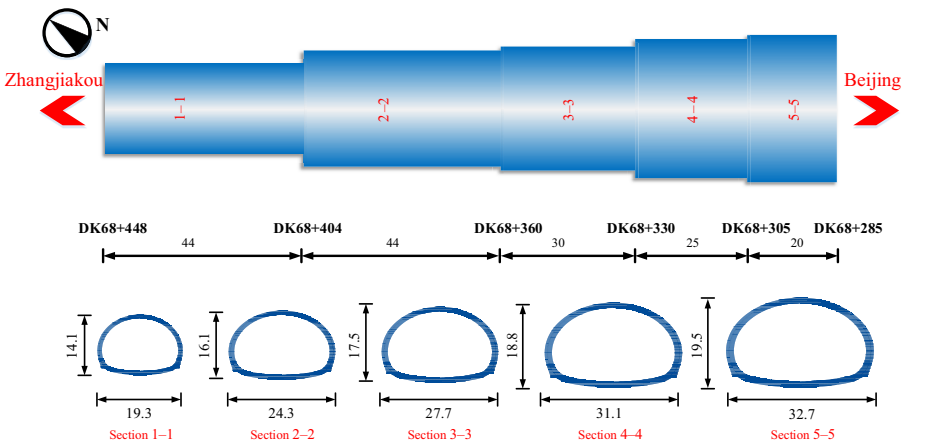

Figure 1.
Plane and section of large-span transition tunnel (Unit: m)

2.2 Microseismic monitoring scheme

Although microseismic monitoring technology has been widely used in tunnel engineering at home and abroad (Zhuang, Tang, Liang, & Ma, 2017; Ma *et al.*, 2016), it is the first time in the world to apply it to the study of excavation damage zone of surrounding rock in large-span high speed railway tunnel, and there is no successful monitoring experience for direct reference. Therefore, through continuous exploration, microseismic monitoring points are set on the surface and around the large-span transition tunnel of Badaling Great Wall Station of Beijing–Zhangjiakou high-speed railway so as to achieve three-dimensional and all-round microseismic monitoring.

2.2.1 Microseismic monitoring system. The hardware of microseismic monitoring system consists of detector, data acquisition instrument, power supply equipment, clock synchronization device, optical fiber switch and data storage and processing system. The network structure of microseismic monitoring system is shown in Figure 2. Microseismic signals are characterized by small magnitude, generally lower than 0 and wide signal frequency range, ranging from several Hertz to several thousand Hertz, so the performance of detector for receiving signals shall be very high (Zhang & Deng, 2016). Single-component and three-component microseismic detectors are adopted as the detector, with high performance characteristics of high sensitivity ($200\ V \cdot (m \cdot s^{-1})^{-1}$) and wide frequency band (4.5–1,000 Hz), etc. 24-channel and 3-channel microseismic acquisition instruments are adopted as data acquisition instrument, with the characteristics of high resolution, high sampling rate (2,000 Hz), high trigger accuracy and low noise, etc. GPS receiver is built in the acquisition instrument to provide accurate time and location information for the instrument.

2.2.2 Layout of measuring points. Nine measuring points numbered 1#–9# are set on the tunnel surface, and a monitoring envelope is formed with 9# point as the center and 80 m as the radius for radiation; drill holes at the measuring points, with the hole depth about 2 m (rock mass is at the bottom of the hole), and the aperture about 100 mm; each hole is equipped with a three-component detector and, meanwhile, externally connected with a three-channel data acquisition instrument and storage battery, and coupled with yellow mud, as shown in Figure 3. Two sections (DK68 + 290 m, DK68 + 440 m) are selected for monitoring around the tunnel, and each section is set with three measuring holes, with a total of six measuring points numbered 1*–6*. Drill holes at measuring points with a hole depth of about 12 m are considered. A three-component detector (1*–3*) at the bottom of the hole and single-component detector (4*–6*) at

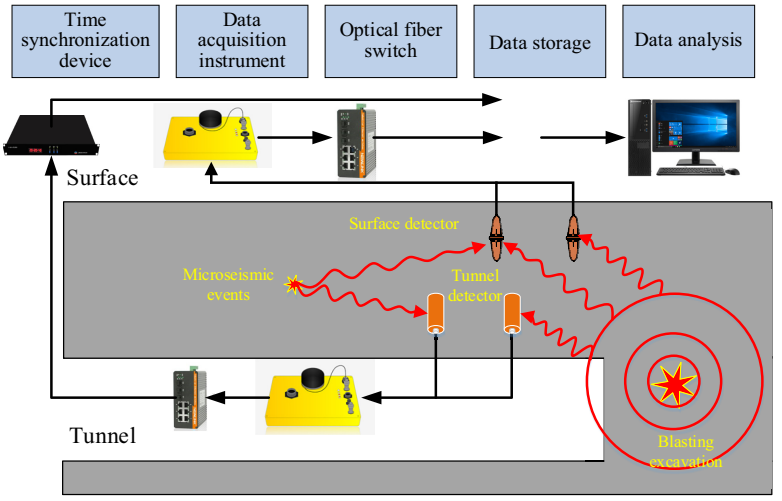

Figure 2.
Schematic diagram of network structure of microseismic monitoring system

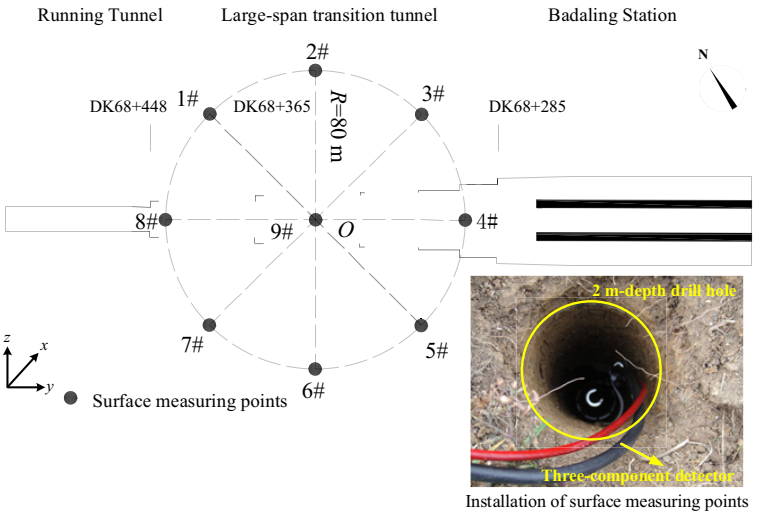

Figure 3.
Layout of surface microseismic measuring points

about 3 m near the tunnel opening are installed, which are coupled by cement grouting, as shown in Figure 4. The measuring points around the tunnel are concentrated, and 12 detectors are connected to the 24-channel data acquisition instrument for centralized signal acquisition. In this way, it is available to ensure that the tunnel blasting excavation is within the monitoring range of the sensor, and the microseismic signals can be continuously received for many times.

2.3 Positioning error

Whether microseismic monitoring can play the role of accurate positioning and prediction of rock mass cracking in tunnel excavation mainly depends on whether the positioning accuracy can meet the engineering requirements, and the positioning error is mainly affected by factors such as the positioning method of microseismic source, the selection value of rock mass wave velocity and the layout mode and number of measuring points (Ma *et al.*, 2016;

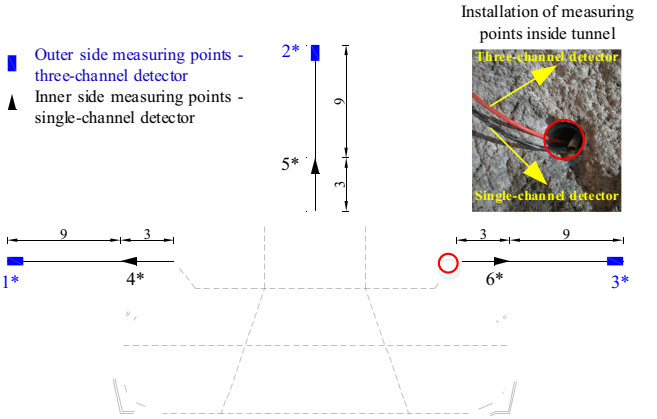

Figure 4.
Layout of microseismic measuring points around the tunnel (DK68 + 290) (Unit: m)

Guo, Dai, Xu, Fan, & Li, 2017). Carrying out the active source excitation test at the microseismic monitoring points and recording the excitation test waveform to realize the rock mass wave velocity calibration of geological field and inversion correction of microseismic source position improves the accuracy of source location.

The monitoring period is from the start of the construction of the large-span transition tunnel to the completion of the primary support construction, and the excavation direction is from large mileage to small mileage. A total of 11,846 microseismic events were monitored during the period, and the distribution of positioning error of microseismic events is as shown in Figure 5. The number of events with the positioning error within 10 m accounts for 72% of all microseismic events, and the number of events with positioning errors within 5 m accounts for 40%, with an average error of 8.05 m. According to the existing research results (Mendecki, 1997; Tang, Liu, Li, Qin, & Xu, 2018), the positioning accuracy of microseismic monitoring can meet the needs of surrounding rock stability evaluation of tunnel and the research of excavation damage zone.

3. Microseismic activity characteristics of large-span transition tunnel

3.1 Moment magnitude distribution of microseismic events

To represent the absolute magnitude of microseismic events, moment magnitude (M) is a widely used magnitude scale at present (Zhuang *et al.*, 2017). The moment magnitude distribution of microseismic events during large-span transition tunnel excavation is shown in Figure 6. It can be seen that the moment magnitude distribution ranges from −3.75 to 0.48, and the average moment magnitude is −1.94. Mostly concentrated in this area, the number of microseismic events with moment magnitude conforming to $-3 \le M \le -1$ accounts for 98% of all microseismic events; of which, $-2 \le M \le -1$ accounts for 66%. According to the moment magnitude distribution, most of the current microseismic events belong to small magnitude events (Zhang *et al.*, 2012).

The research shows that within a certain time range, microseismic events follow the relational expression of moment magnitude and frequency (Zhang & Deng, 2016).

$$lgN = a - bM \tag{1}$$

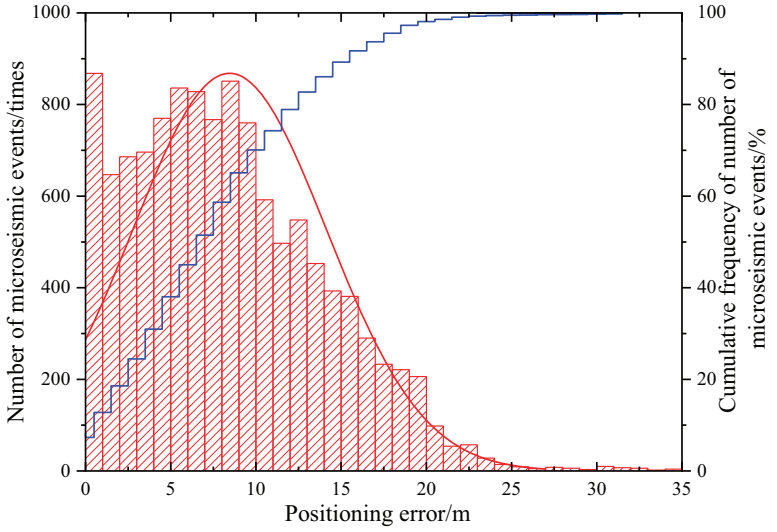

Figure 5.
Positioning error distribution of microseismic events

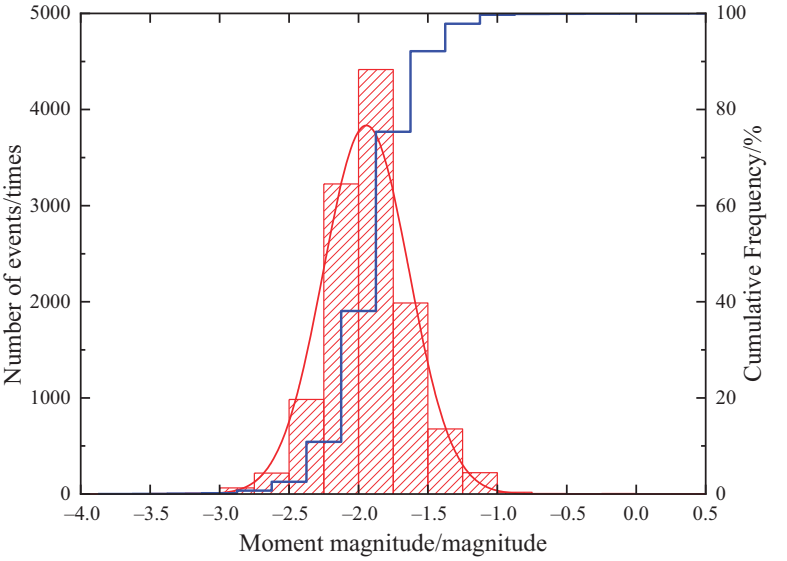

Figure 6.
Moment magnitude distribution of microseismic events

where N is the number of events with moment magnitude greater than or equal to M; a and b are constants.

Constant a represents the microseismic activity level in statistical time and region. The constant B value represents the function of the relative magnitude distribution of microseismic events. The smaller the b value is, the more events with great moment magnitude are. At the same time, the change of b value can be used to reflect the change of stress field. In case of microseismic activity of fault slip type, corresponding b value is usually smaller than 0.8, while in case of microseismic activity of blasting induced stress migration type, corresponding b value is usually between 1.2 and 1.5 (Xu, Dai, Zhou, Sha, & Tang, 2014). Fit the monitored microseismic events data to get $a = 0.8$ and $b = 1.5$, as shown in Figure 7. It can be seen that the regularity of microseismic event activity is good, and the microseismic activity in the monitored area is mainly blasting induced stress migration type.

3.2 Spatial distribution of microseismic events

The moment magnitude distribution of microseismic events around the tunnel is shown in Figure 8a, in which spheres represent microseismic events, and the size and different colors of spheres represent the moment magnitude of microseismic events. It can be seen that microseismic events are mainly concentrated on both sides of the tunnel, and the closer to the tunnel, the greater the magnitude of microseismic events. The microseismic events with the largest moment magnitude are mainly concentrated near the tunnel of Class V surrounding rock, which indicates that when the class of surrounding rock is poor, more energy will be released during the cracking of rock mass, and the cracking size of rock mass will be larger. The plane distribution of density of microseismic events is as shown in Figure 8b. Different colors in the figure represent relative distribution density of microseismic events. It can be seen that the closer to both sides of the tunnel, the greater the relative density of microseismic events and the more concentrated the microseismic events.

The distribution density of microseismic events in the cross-section of tunnel (taking DK68 + 400 section as an example) is shown in Figure 9. It can be seen that microseismic

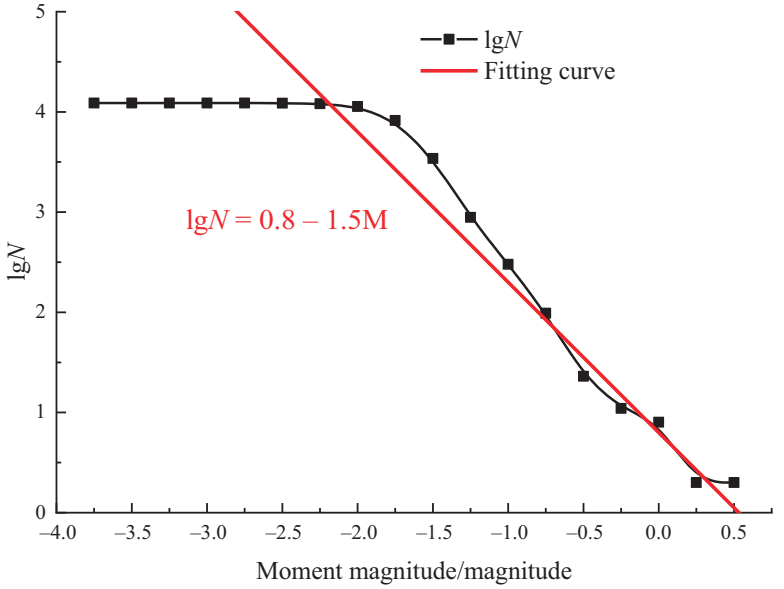

Figure 7.
Moment magnitude–frequency distribution of microseismic events

events are mainly concentrated around the tunnel, and the closer to the tunnel, the greater the density of microseismic events, and the density of microseismic events at the arch crown is the largest and that at the arch bottom is smaller. Therefore, according to the distribution density of microseismic events, the distribution map of microseismic events can be divided into three areas, namely high density area, medium density area and low density area of microseismic events.

3.3 Zoning index of microseismic events

The spatial distribution characteristics of microseismic events in large-span tunnel are quantitatively analyzed through distribution frequency and cumulative distribution frequency of microseismic events. The distribution frequency of microseismic events refers to the ratio of the number of microseismic events within a certain depth range at a certain position of a tunnel to the number of all microseismic events at the position.

For the tunnel of the same section form, the distribution frequencies of microseismic events at the left haunch, right haunch, arch crown and arch bottom of the tunnel are, respectively, provided. The distribution frequency of microseismic events at the left haunch and right haunch of the tunnel with section 1-1 is as shown in Figure 10. It can be seen from the figure that the distribution frequency of microseismic events in high density area is higher and stably above 20%, the frequency of microseismic events in medium density areas decreases somewhat and the frequency of microseismic events in low density area is lower with the stable value lower than 10%. The results can also verify the rationality of the three areas proposed qualitatively above. The cumulative distribution frequency of microseismic events refers to the ratio of the number of microseismic events occurred between the tunnel boundary and a certain depth position to the total number of microseismic events. The higher slope of the cumulative distribution frequency curve indicates that the cumulative distribution frequency increases faster, and the concentrated area of microseismic events is smaller; when the slope of cumulative distribution frequency remains unchanged, it indicates that the distribution

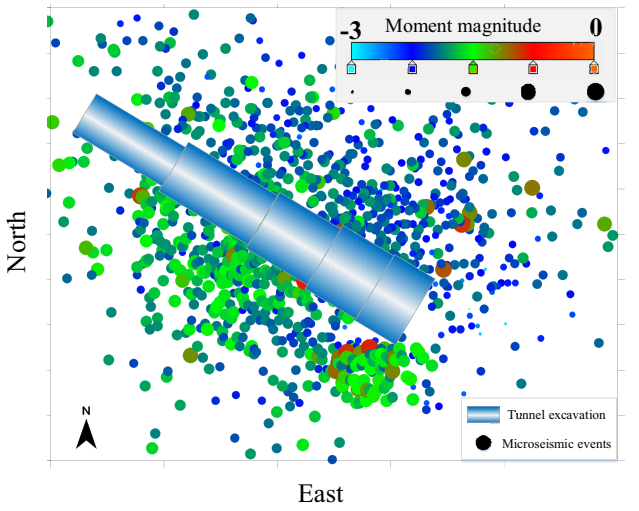

Moment magnitude distribution of microseismic events (10% of all microseismic events)

(a)

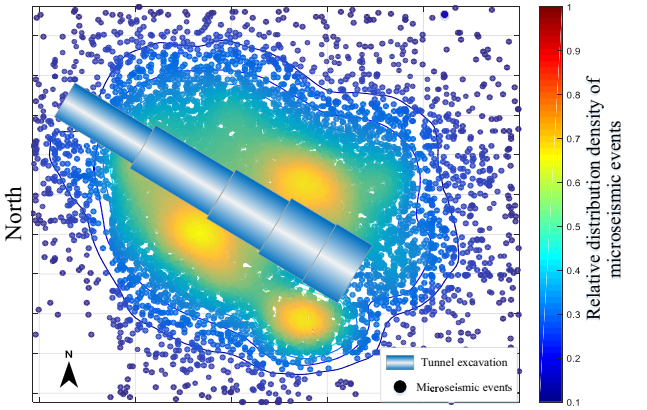

Distribution density of microseismic events (all microseismic events)

(b)

Figure 8.
Plane distribution of microseismic events

characteristics of microseismic events in the area are consistent; when the slope of the cumulative distribution frequency curve changes, it indicates that there are obvious differences in the distribution characteristics of microseismic events in the area.

The distribution frequency and cumulative distribution frequency of microseismic events in the large-span transition tunnel under five section forms are as shown in Figures 11 and 12. It can be seen from the figure that the cumulative distribution frequency of high density area is about 60% and that of medium density area is about 80%. Therefore, the positions of the three areas of microseismic events are defined quantitatively: The boundary where the

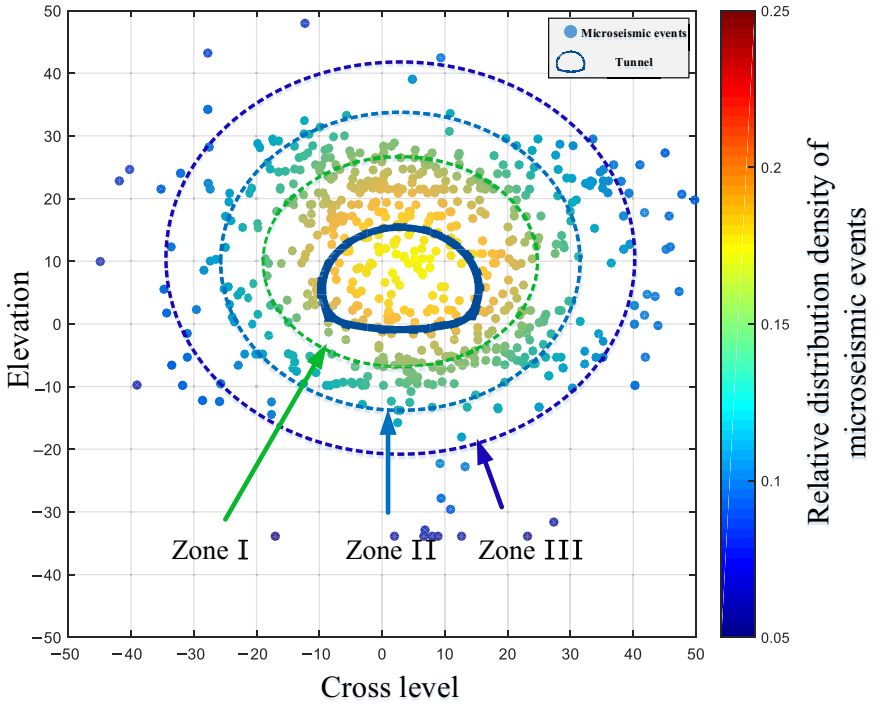

Figure 9.
Cross-section density distribution of microseismic events

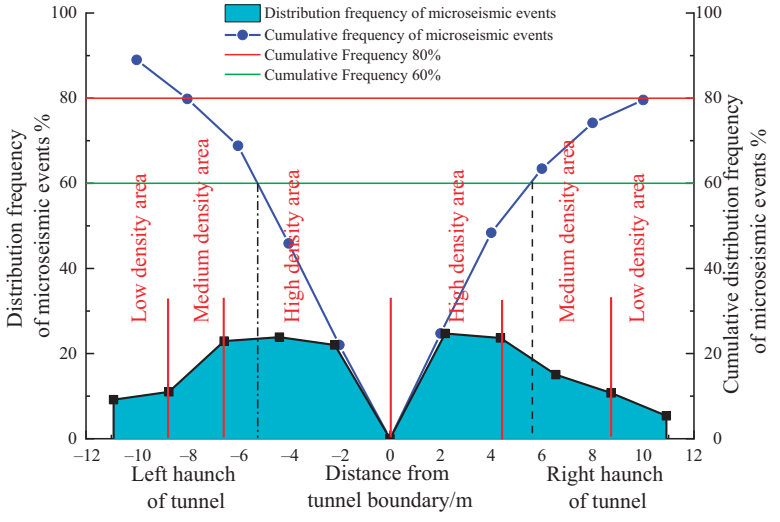

Figure 10.
Distribution frequency of microseismic events at the left haunch and right haunch of the tunnel (section 1-1)

cumulative distribution frequency of microseismic events is 60% is the junction of high density area and medium density area; the boundary where the cumulative distribution frequency is 80% is the junction of medium density area and low density area.

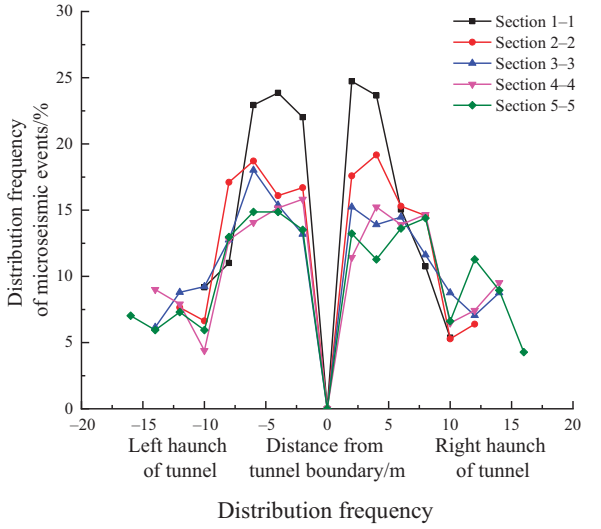

Figure 11.
Distribution of microseismic events at the left haunch and right haunch of the tunnel

4. Characteristics of excavation damage zone in surrounding rock of large-span transition tunnel

4.1 Depth of excavation damage zone of surrounding rock

The reason for excavation damage of surrounding rock is that excavation disturbance causes a large number of tiny cracks in rock mass, so the damage degree of surrounding rock is consistent with the density of cracks in rock mass. The more cracks in rock mass, the higher the damage degree of the surrounding rock. According to the different damage and

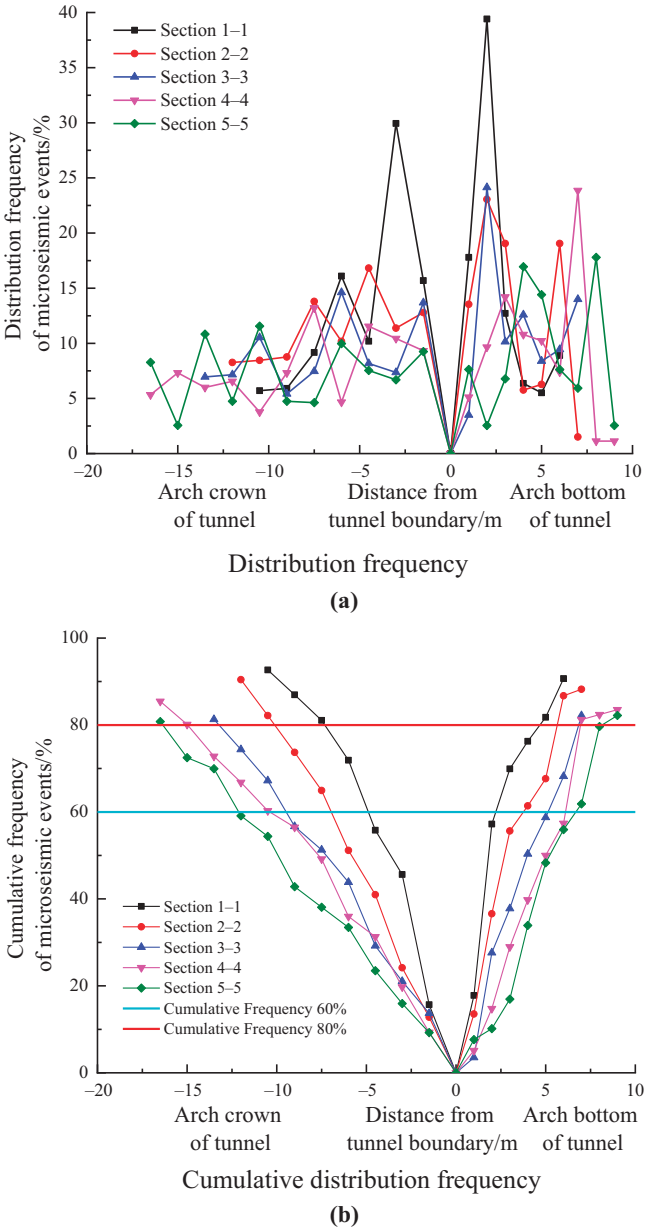

Figure 12.
Distribution of microseismic events at arch crown and arch bottom of the tunnel

disturbance degree of surrounding rock after excavation (Liu *et al.*, 2013; Dai *et al.*, 2015), the surrounding rock is divided into high excavation damage zone, low excavation damage zone and excavation disturbance zone successively. Therefore, the high density area, medium density area and low density area of microseismic events can be corresponded to the high excavation damage zone, low excavation damage zone and excavation disturbance zone of

surrounding rock, respectively. In a short period of time after tunnel excavation, with the stress adjusting of surrounding rock the high excavation damage zone of surrounding rock near the tunnel is generated, and the scope and degree of the damage zone have a tendency of further expansion. Therefore, it is necessary to restrain the high damage zone of surrounding rock effectively in time (Martino & Chandler, 2004; Chen *et al.*, 2010) so as to inhibit the development of the high damage zone of surrounding rock and ensure the safety of tunnel construction.

According to the distribution frequency characteristics of microseismic events in large-span tunnels (Figures 11 and 12), the summary table on the depth of high excavation damage zone of surrounding rock in different positions of the tunnel under five section forms can be obtained, as shown in Table 1. In order to analyze the factors influencing the depth of high damage zone of surrounding rock, the ratio β of the depth of high excavation damage zone (l_{HDZ}) to the span (W) of surrounding rock with different classes is calculated, and the relationship diagram between β and surrounding rock class is obtained, as shown in Figure 13.

It can be seen from Figure 13 that the depth of high excavation damage zone of surrounding rock is greatly affected by location, and the depth of high damage zone of

Table 1.
Summary of depth of high damage zone of surrounding rock in long-span transition tunnel

Section	Class of surrounding rock	Depth of high damage zone of surrounding rock/m			
		Arch crown	Arch bottom	Left haunch	Right haunch
1-1	III	4.9	2.2	5.2	5.6
2-2	III	7.2	4.0	7.0	7.1
3-3	IV	9.5	5.1	8.1	9.1
4-4	IV	10.5	6.1	8.9	9.6
5-5	V	12.1	6.8	9.2	10.1

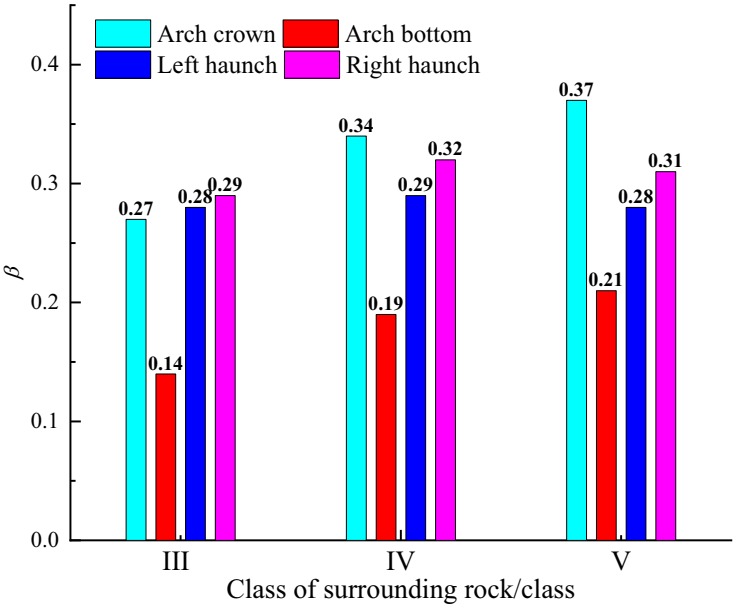

Figure 13.
Relationship between high damage zone β of surrounding rock and surrounding rock class in different positions of tunnel

surrounding rock generally shows the trend of arch crown > right haunch > left haunch > arch bottom; under the conditions of three surrounding rock classes, β value at the position of left haunch and right haunch of the tunnel is relatively concentrated, which is 0.28–0.29 and 0.29–0.32, respectively, indicating that the value at the position of left haunch and right haunch is less affected by the class of surrounding rock. Therefore, the prediction formulas for depth of high damage zone of surrounding rock at the position of left haunch and right haunch are as follows:

$$l_{\text{HDZ left haunch}} = 0.285W \tag{2}$$

$$l_{\text{HDZ right haunch}} = 0.305W \tag{3}$$

The β value at the position of arch crown and arch bottom is greatly affected by the class of surrounding rock. With the deterioration of surrounding rock conditions, the β value increases obviously, and the variation ranges are 0.27–0.37 and 0.14–0.21, respectively. Therefore, considering the influence of tunnel span and class of surrounding rock (C), the prediction formulas for the depth of high damage zone of surrounding rock at the position of arch crown and arch bottom are as follows:

$$l_{\text{HDZ arch crown}} = (0.13 + 0.05C)W \tag{4}$$

$$l_{\text{HDZ arch bottom}} = (0.03 + 0.035C)W \tag{5}$$

The predicted value and the measured value of the depth of surrounding rock are compared at different positions of the large-span tunnel to get the average value of relative error between the predicted value and measured value of Formulas (2)–(5), which is 2.14, 3.91, 4.83 and 11.70%, respectively. The average value of relative error of the prediction formulas for arch crown and the left and right haunches is lower than 5%, and the average value of relative error of the prediction formula for arch bottom is too large, which is caused by the great distance of the installation position of detector away from the arch bottom of tunnel and the high microseismic positioning error. The results show that the prediction formula for the depth of high damage zone of surrounding rock in different positions of long-span tunnel is of high accuracy.

4.2 Damage degree of excavation damage zone of surrounding rock

In addition to the depth of damage zone, the characteristics of excavation damage zone of surrounding rock also include the damage degree of excavation damage zone (Liu *et al.*, 2013). When the depth of excavation damage zone of surrounding rock is constant, the difference of damage characteristics of surrounding rock is mainly manifested by the difference of damage degree, that is, the scale of internal crack initiation and slip in the damage zone. Tunnel blasting or excavation disturbance causes stress concentration and cracking of rock mass, and there will be a certain amount of slip along the fracture surface. As the energy released by rock mass cracking is different, the crack length and slip amount will also be different. The average moment magnitude of microseismic events represents the amount of energy released during rock mass cracking in a certain area, so the moment magnitude has a strong correlation with the parameters, such as cracking size and slip length in rock mass (Goodfellow & Young, 2014), as shown in Figure 14. It can be seen that the larger the average moment magnitude of microseismic events, the larger the cracking size and slip, which increases the damage degree of rock mass. When the fracture size and slip length of rock mass reach a certain degree, local rock mass may fall off, further resulting in collapse accident. Therefore, the damage degree of surrounding rock can be scaled by the average moment magnitude parameter of microseismic events. For microseismic events with larger moment magnitude, the location and inducing factors shall be analyzed to ensure the safety of tunnel construction.

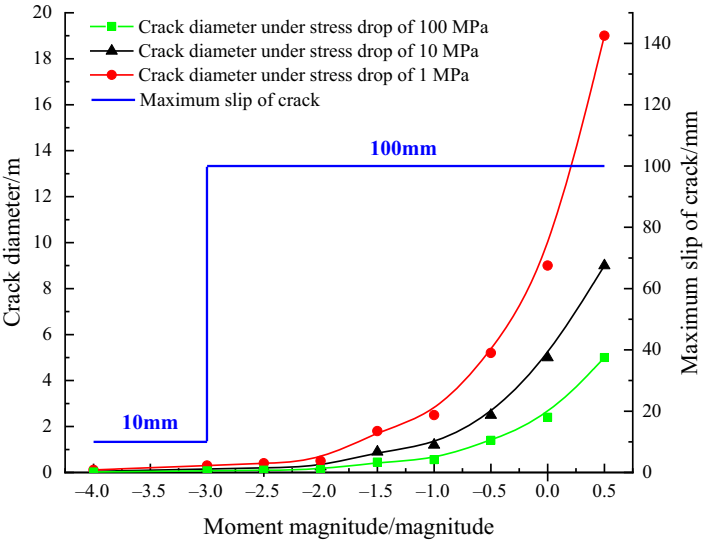

Figure 14.
Relationship between moment magnitude and cracking size and slip length

According to the monitoring results of microseismic events, the average moment magnitude of microseismic events in five section forms of large-span tunnels under different classes of surrounding rock is obtained, and its relationship with tunnel span and class of surrounding rock is as shown in Figure 15. It can be seen from the figure that for the same class of surrounding rock (Class III and IV), with the increase of tunnel span, the average moment magnitude of microseismic events changes slightly, but with the weakening of surrounding rock conditions from Class III to Class V, the average moment magnitude of microseismic events increases significantly, so the damage degree of surrounding rock damage zone is greatly affected by the class of surrounding rock and less affected by the tunnel excavation span.

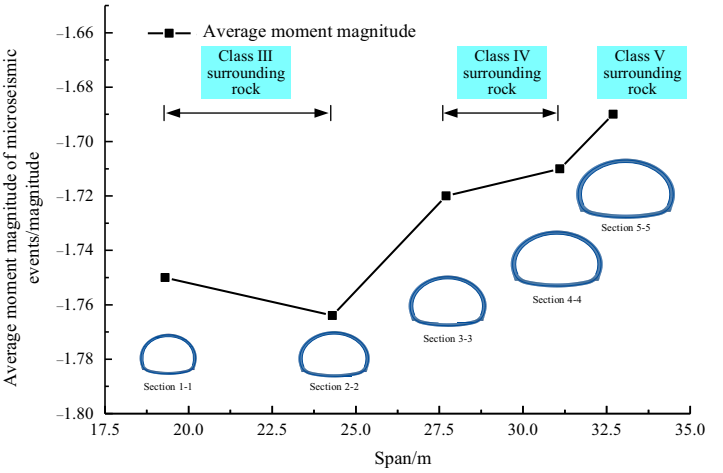

Figure 15.
Relationship between average moment magnitude of microseismic events and tunnel span and class of surrounding rock

5. Relationship between excavation damage zone and deformation of surrounding rock in large-span tunnel

The cracking of rock mass will be accompanied by the emergence and development of crack deformation (Wang *et al.*, 2018). The relationship between the depth of high damage zone of surrounding rock and the settlement of tunnel arch crown and convergence of haunch can be obtained by setting deformation measuring points at the arch crown and left and right haunches of tunnel under five section forms, as shown in Figure 16, from which the following conclusions can be drawn.

(1) The depth of high damage zone of surrounding rock at arch crown and left and right haunches is positively correlated with the settlement of arch crown and convergence of haunch, and the correlation is strong. A larger depth of damaged zone of surrounding rock will inevitably lead to a larger deformation of surrounding rock. Therefore, the depth of high damage zone of surrounding rock can be predicted according to the deformation of surrounding rock to judge whether the current supporting measures are effective or not.

(2) The relationship between the depth and deformation of high excavation damage zone of surrounding rock presents obvious stage characteristics. Taking the relationship between the depth and deformation of high damage zone of surrounding rock at arch crown as an example, the abscissa value and the ordinate value of points A, B, C, D and E in Figure 16a correspond to the depth and settlement of high damage zone of surrounding rock at the arch crown of tunnel under five section forms, respectively. When the depth of damaged zone is small (points A, B and C), the slope of surrounding rock deformation is small, and when the depth of damaged zone is large (points C, D and E), the slope of surrounding rock deformation increases obviously, which indicates that when the depth of damage zone is small, the overall stability of surrounding rock is strong, which can effectively inhibit deformation, and when the depth of the damage zone is large, the self-stability of surrounding rock is weak, and the inhibiting ability to deformation is lower.

(3) The increase of deformation does not mean that the damage zone of surrounding rock is infinitely expanded (from point E), and the damage zone of surrounding rock is limited under certain conditions. The reason is that the surrounding rock has the ability of self-arching, and the excavation disturbance is mainly concentrated in the bearing arch of the surrounding rock, which causes damage to the rock mass inside the bearing arch and has little influence on the surrounding rock outside the bearing arch. However, when the damage of surrounding rock in the bearing arch develops to a certain extent, there will be a tendency of relaxation and collapse, and the deformation will increase sharply until collapse occurs.

6. Anchor cable (rod) parameter design in large-span transition tunnel

The range and distribution of excavation damage zone of surrounding rock directly affects the stability of surrounding rock, so it is an important basis for tunnel support design. For prestressed anchor cable (rod), the anchored section is required to be in stable rock mass, so the designed length of free end (L_f) of prestressed anchor cable (rod) shall be greater than the depth of damage zone of surrounding rock (l_{HDZ}). The excavation damage zone of surrounding rock includes high damage zone and low damage zone, and there is obvious difference in damage crack density between them. The crack distribution in low damage zone is less, which indicates that there is local undamaged zone in low damage zone, and the surrounding rock does not completely lose its bearing capacity (Liu *et al.*, 2015). Using anchor

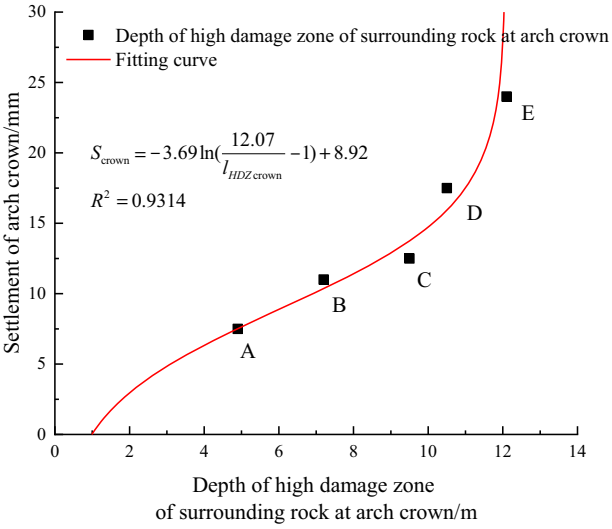

Relationship between the depth of high damage zone of surrounding rock at arch crown and settlement of arch crown

(a)

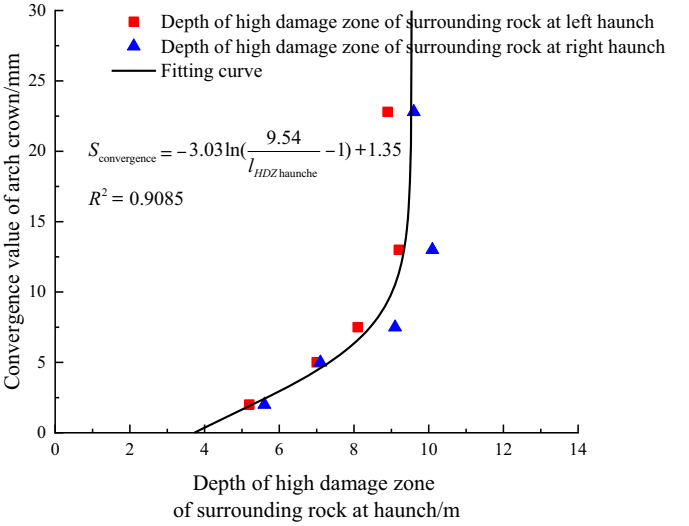

Relationship between the high damage zone of surrounding rock at left and right haunches and the convergence value of haunch

(b)

Figure 16.
Relationship between depth of high damage zone of surrounding rock and settlement of arch crown and convergence value of haunch

cable (rod) to pass through the high damage zone of surrounding rock and enter the low damage zone to a certain depth can also meet the needs of ensuring the stability of surrounding rock.

In order to meet the requirement of 300 years' design service life of large-span transition tunnel, according to the depth of high damage zone of surrounding rock (see Table 1) and considering the overall sliding deformation of anchor cable (rod), a certain safety margin shall be reserved in the design of prestressed anchor cable (rod), so the designed anchor cable (rod) parameters of large-span transition tunnel are shown in Table 2. Based on the comparison of Table 1 and 2, it can be seen that the design length of the free segment of prestressed anchor cable of the large-span transition tunnel is enough to pass through the whole high damage zone of surrounding rock. Taking section 1-1 as an example, the length of the free segment of anchor cable (9 m) is much greater than the depth (5.6 m) of the high damage zone of surrounding rock (at the right haunch). Upon completion of tunnel excavation, the deformation of surrounding rock is controlled within 30 mm, which indicates that the anchor cable (rod) support passing through the high excavation damage zone of surrounding rock can effectively control the development of the high damage zone of surrounding rock, make the deformation of surrounding rock smaller and ensure the safety of tunnel construction.

7. Conclusion

(1) According to the spatial distribution density characteristics of microseismic events, the microseismic events around the tunnel are divided into three areas: high density area, medium density area and low density area, and their positions are quantified according to the cumulative distribution frequency of microseismic events. The boundary with 60% cumulative distribution frequency of microseismic events can be used as the junction of high density area and medium density area, and the boundary with 80% cumulative distribution frequency can be used as the junction of medium density area and low density area.

(2) The high, medium and low density areas of microseismic events are correspondingly defined as high excavation damage zone, low excavation damage zone and excavation disturbance zone of surrounding rock. The influence of surrounding rock class and tunnel span on the depth of high excavation damage zone of surrounding rock is analyzed, and the prediction formula for the depth of high excavation damage zone of surrounding rock at different positions of the tunnel is given. The average moment magnitude of microseismic events is taken as a direct parameter reflecting the damage degree of surrounding rock.

(3) There is a strong positive correlation between the depth of the high excavation damage zone of surrounding rock and the deformation of surrounding rock, as well as

	Anchor rod		Anchor cable	
Section	Free segment length/m	Anchored section length/m	Free segment length/m	Anchored section length/m
1-1	6	3	9	6
2-2				
3-3	7		14	
4-4				
5-5	8		19	

Table 2. Anchor cable (rod) design parameters of large-span transition tunnel

obvious stage characteristics, so the damage zone can be predicted according to the deformation of surrounding rock.

(4) Anchor cable (rod) parameter design is carried out according to the depth of high damage zone of surrounding rock to ensure that the free segment of prestressed anchor cable passes through the whole high damage zone. The deformation results of surrounding rock show that the high excavation damage zone of surrounding rock is effectively inhibited, which ensures the construction safety.

References

Cai, M., & Kaiser, P. K. (2005). Assessment of excavation damaged zone using a micromechanics model. *Tunnelling and Underground Space Technology*, *20*(4), 301–310.

Cai, M., Kaiser, P. K., & Martin, D. (2001). Quantification of rock mass damage in underground excavations from microseismic event monitoring. *International Journal of Rock Mechanics and Mining Sciences*, *38*(8), 1135–1145.

Chen, B., Feng, X., Xiao, Y., Ming, H., Zhang, C., Hou, J. & Chu, W. (2010). Acoustic emission test on damage evolution of surrounding rock in deep-buried tunnel during TBM excavation. *Chinese Journal of Rock Mechanics and Engineering*, *29*(8), 1562–1569, In Chinese.

Dai, F., Li, B., Xu, N., Zhu, Y., Sha, C., Xiao, P., & He, G. (2015). Characteristics of damaged zones due to excavation in deep underground powerhouse at houziyan hydro power station. *Chinese Journal of Rock Mechanics and Engineering*, *34*(4), 735–746, In Chinese.

Goodfellow, S. D., & Young, R. P. (2014). A laboratory acoustic emission experiment under in situ conditions. *Geophysical Research Letters*, *41*(10), 3422–3430.

Guo, L., Dai, F., Xu, N., Fan, Y., & Li, B. (2017). Research on msfm-based microseismic source location of rock mass with complex velocities. *Chinese Journal of Rock Mechanics and Engineering*, *36*(2), 394–406, In Chinese.

Li, Z., Shigenori, Y., Koji, H., Hisaya, Y., & Hideo, K. (2001). Study of estimation of loosened region around rock cavern by acoustic emission technique. *Chinese Journal of Rock Mechanics and Engineering*, *20*(Supplement 1), 1177–1181, In Chinese.

Li, Y., Liu, J., Zhao, X., & Yang, Y. (2009). Study of *b*-value and fractal dimension of acoustic emission during rock failure process. *Rock and Soil Mechanics*, *30*(9), 2559–2563, In Chinese.

Liu, N., Zhang, C., Chen, X., Hou, J., & Chu, W. (2011). Monitoring and characteristics study of stress evolution of surrounding rock during deep tunnel excavation. *Chinese Journal of Rock Mechanics and Engineering*, *30*(9), 1729–1737, In Chinese.

Liu, N., Zhang, C., Chu, W., & Wu, X. (2013). Excavation damaged zone characteristics in deep tunnel of Jinping II hydropower station. *Chinese Journal of Rock Mechanics and Engineering*, *32*(11), 2235–2241, In Chinese.

Liu, N., Zhang, C., & Chu, W. (2015). Depth of fracture and damage in deep-buried surrounding rock and bolt length design. *Chinese Journal of Rock Mechanics and Engineering*, *34*(11), 2278–2284, In Chinese.

Ma, K., Tang, C., Liang, Z., Wu, J., Xu, N., & Zhuang, D. (2016). Stability analysis of the surrounding rock of underground water-sealed oil storage caverns based on microseismic monitoring during construction. *Chinese Journal of Rock Mechanics and Engineering*, *35*(7), 1353–1365, In Chinese.

Martin, D. (1997). Seventeenth Canadian Geotechnical Colloquium: The effect of cohesion loss and stress path on brittle rock strength. *Canadian Geotechnical Journal*, *34*(5), 698–725.

Martino, J. B., & Chandler, N. A. (2004). Excavation-Induced damage studies at the underground research laboratory. *International Journal of Rock Mechanics and Mining Sciences*, *41*(8), 1413–1426.

Mendecki, A. J. (1997). *Seismic Monitoring in Mines*. London: Chapman and Hall Press.

Read, R. S. (2004). 20 years of excavation response studies at AECL's underground research laboratory. *International Journal of Rock Mechanics and Mining Sciences*, *41*(8), 1251–1275.

Sato, T., Kikuchi, T., & Sugihara, K. (2000). In-situ experiments on an excavation disturbed zone induced by mechanical excavation in Neogene sedimentary rock at Tono mine, central Japan. *Engineering Geology*, *56*(1/2), 97–108.

Tang, Z., Liu, X., Li, C., Qin, P., & Xu, Q. (2018). Microseismic characteristic analysis in deep TBM construction tunnels. *Journal of Tsinghua University: Science and Technology*, *58*(5), 461–468, In Chinese.

Wang, L., Wang, Q., Li, S., Xu, N., Pan, R., He, M., *et al.* (2018). Stability analysis and characteristic of seismic activity during roadway development in soft rock. *Journal of Mining and Safety Engineering*, *35*(1), 10–18.

Xu, N., Dai, F., Zhou, Z., Sha, C., & Tang, C. (2014). Study of characteristics of *b* value for microseismic events in high rock slope. *Chinese Journal of Rock Mechanics and Engineering*, *33*(Supplement 1), 3368–3374, In Chinese.

Zhang, B., & Deng, J. (2016). *Microseismic Mechanism of Engineering Rock Mass and its Application*. Beijing: Science Press.

Zhang, B., Deng, J., Zhou, Z., Lü, H., Wu, J., & Wu, S. (2012). Analysis of monitoring microseism in areas controlled by faults near powerhouse in Dagangshan hydropower station. *Rock and Soil Mechanics*, *33*(Supplement 2), 213–218, In Chinese.

Zhang, M., Lü, G., Jiao, Y., Liu, J., Luo, D., & Peng, F. (2018). A new technique of high-performance and fast tensioning prestressed anchorage cable. *Journal of Railway Engineering Society*, *35*(11), 72–76, In Chinese.

Zhu, Z., Sheng, Q., Zhang, Y., & Li, Y. (2013). Research on excavation damage zone of underground powerhouse of Dagangshan hydropower station. *Chinese Journal of Rock Mechanics and Engineering*, *32*(4), 734–739, In Chinese.

Zhuang, D., Tang, C., Liang, Z., & Ma, K. (2017). Reinforcement effect of anti-shear tunnels of Dagangshan right bank slope based on microseismic energy evolution. *Chinese Journal of Geotechnical Engineering*, *39*(5), 868–878, In Chinese.

Corresponding author
Ao Li can be contacted at: 15115279@bjtu.edu.cn